PLOS ONE

RESEARCH ARTICLE

Systematic multiscale models to predict the compressive strength of fly ash-based geopolymer concrete at various mixture proportions and curing regimes

Hemn Unis Ahmed[1], **Ahmed Salih Mohammed**[1]*, **Azad A. Mohammed**[1], **Rabar H. Faraj**[2]

1 Department of Civil Engineering, College of Engineering, University of Sulaimani, Sulaimaniyah, Iraq,
2 Civil Engineering Department, University of Halabja, Halabja, Kurdistan Region, Iraq

* ahmed.mohammed@univsul.edu.iq

Citation: Ahmed HU, Mohammed AS, Mohammed AA, Faraj RH (2021) Systematic multiscale models to predict the compressive strength of fly ash-based geopolymer concrete at various mixture proportions and curing regimes. PLoS ONE 16(6): e0253006. https://doi.org/10.1371/journal.pone.0253006

Editor: Tianyu Xie, RMIT University, AUSTRALIA

Received: February 7, 2021

Accepted: May 26, 2021

Published: June 14, 2021

Peer Review History: PLOS recognizes the benefits of transparency in the peer review process; therefore, we enable the publication of all of the content of peer review and author responses alongside final, published articles. The editorial history of this article is available here: https://doi.org/10.1371/journal.pone.0253006

Data Availability Statement: All relevant data are within the manuscript.

Funding: The authors received no specific funding for this work.

Abstract

Geopolymer concrete is an inorganic concrete that uses industrial or agro by-product ashes as the main binder instead of ordinary Portland cement; this leads to the geopolymer concrete being an eco-efficient and environmentally friendly construction material. A variety of ashes used as the binder in geopolymer concrete such as fly ash, ground granulated blast furnace slag, rice husk ash, metakaolin ash, and Palm oil fuel ash, fly ash was commonly consumed to prepare geopolymer concrete composites. The most important mechanical property for all types of concrete composites, including geopolymer concrete, is the compressive strength. However, in the structural design and construction field, the compressive strength of the concrete at 28 days is essential. Therefore, achieving an authoritative model for predicting the compressive strength of geopolymer concrete is necessary regarding saving time, energy, and cost-effectiveness. It gives guidance regarding scheduling the construction process and removal of formworks. In this study, Linear (LR), Non-Linear (NLR), and Multi-logistic (MLR) regression models were used to develop the predictive models for estimating the compressive strength of fly ash-based geopolymer concrete (FA-GPC). In this regard, a comprehensive dataset consists of 510 samples were collected in several academic research studies and analyzed to develop the models. In the modeling process, for the first time, twelve effective variable parameters on the compressive strength of the FA-GPC, including SiO_2/Al_2O_3 (*Si/Al*) of fly ash binder, alkaline liquid to binder ratio (*l/b*), fly ash (*FA*) content, fine aggregate (*F*) content, coarse aggregate (*C*) content, sodium hydroxide (*SH*)content, sodium silicate (*SS*) content, (*SS/SH*), molarity (*M*), curing temperature (*T*), curing duration inside ovens (*CD*) and specimen ages (*A*) were considered as the modeling input parameters. Various statistical assessments such as Root Mean Squared Error (RMSE), Mean Absolute Error (MAE), Scatter Index (SI), OBJ value, and the Coefficient of determination (R^2) were used to evaluate the efficiency of the developed models. The results indicated that the NLR model performed better for predicting the compressive strength of FA-GPC mixtures compared to the other models. Moreover, the sensitivity analysis demonstrated that the curing temperature, alkaline liquid to binder ratio, and sodium

Competing interests: The authors have declared that no competing interests exist.

silicate content are the most affecting parameter for estimating the compressive strength of the FA-GPC.

1. Introduction

It is commonly known that the production of Portland cement (PC) needs a considerable amount of energy as well as participates in about 7% of the total volume of carbon dioxide in the atmosphere. In the cement factories, around 50% of carbon dioxide is directly released into the air when the limestone heated in the calcination process, 40% delivers to the atmosphere as a result of the combustion of fuels to heat the rotary kiln, and the remaining 10% of the released carbon dioxide is measured for quarrying and transporting [1,2]. Also, around 2.8 tons of raw materials are needs for the manufacture of one ton of cement; this is a resource-exhausting process that consumes a large number of natural resources such as limestone and shale for the production of clinkers for cement [3]. Furthermore, approximately one trillion liters of mixing water are required to be used in the concrete industry annually [4]. In the same context, after the steel and aluminum industry, cement is one of the most energy-exhaustive construction materials that used around 110–120 kWh to produce one ton of cement in a typical cement plant alone [5].

Nevertheless, the majority of the cementing materials for the production of concrete are PC. Therefore, to decrease PC's environmental impact, a lot of research has been carried out to develop a new material to be an alternative to the PC [6]; geopolymer technology was developed first by Davidovits in France 1970 [7]. The green gas emission of geopolymer concrete (GC) is around 70% lower than the PC concrete due to the high consumption of waste materials in the mix proportions of the GC [8].

Geopolymers are one of the parts of mineral alumino-silicate polymers that generated from alkaline activation of different materials that rich in aluminosilicate materials, such as natural materials like metakaolin, by-product industrial materials like fly ash (FA), and the by-product of agro materials such as rice husk ash (RHA) [9]. The microstructure of geopolymer materials is amorphous and their chemical constituents are similar to the natural zeolitic materials. The mineral composition of the ash-based geopolymer and alkaline activators are the factors that affect the final product of the polymerization process. Also, the high temperature has usually accelerated the polymerization process [10,11]. So it can be concluded that geopolymer is the third generation of cementing materials after lime and cement [12]. Geopolymer concrete is a mixture of aluminosilicate binder, aggregates, alkaline solution, and water. Binder source materials such as FA, RHA, Ground Granulated Blast Furnace Slag (GGFBS), and metakaolin, or any hybridization between these ashes with or without PC. The most common industrial waste used as cementing material is FA, and it is divided into two classes: class F fly ash and Class C fly ash. The former FA has lower calcium content than class C FA [13]; FA has a variety of applications with high and low volumes for the production of different cementitious composites [14]. Aggregates consist of fine and coarse particles with required properties and gradation. The alkaline solution is a mixture of sodium hydroxide or potassium hydroxide with sodium silicate or potassium silicate. The polymerization between these ingredients produces a solid concrete almost like normal concrete [15].

The polymerization mechanism could be briefly explained as follows; in the first stage, dissolution of the silicate and aluminum elements of the binder inside the high alkalinity aqueous solution produces ions of silicon and aluminum oxide. In the second stage, a mixture of silicate, aluminate, and aluminosilicate species, which through a contemporaneous operation of

poly-condensation-gelation further condensation, finally produces an amorphous gel [16]. Several factors could influence the performance of GC such as type of binder, the concentration of the alkaline solution, the molarity of sodium hydroxide, sodium silicate to sodium hydroxide ratio, extra water, mix proportion, and curing method [17].

Compressive strength of all types of concrete composites, including GC is one of the most remarkable mechanical properties. Usually, it gives a general performance about the quality of the concrete composites [18]. The compressive strength test is conducted by following the standard test methods of ASTM C39 or BS EN 12390–3 [19,20]. In the literature, a variety of studies have been conducted to investigate the influence of several mixture parameters on the mechanical properties of FA-GPC, for instance, Hardjito et al., [21] studied the influence of different parameters such as molarity, sodium silicate to sodium hydroxide ratio, curing temperature, curing time, the dosage of high range water-reducing admixture, handling time, the water content in the mixture and age of concrete on the compressive strength of GC. They revealed that the higher molarity, sodium silicate to sodium hydroxide ratio, higher curing temperatures, and curing time gives higher compressive strength to the GC; At the same time, the increment in the percent of water leads to a reduction in the compressive strength [21].

On the other hand, a research study has been carried out by Patankar et al. [22] on the effect of water to geopolymer binder ratio on the performance of FA-GPC. They observed that the compressive strength was declined as the water to geopolymer binder ratio increased [22]. Similar observations can also found in other studies even though different mixture proportions were used [23].

One of the factors that affect the polymerization process is the type and quantity of the alkaline liquids by influencing the release of Si^{4+} and Al^{3+} from the base binders. Alkaline liquids of greater concentration are usually beneficial for getting higher compressive strength up to an optimal range [24]. Singhal et al. [25] prepared FA-GPC with different sodium hydroxide concentrations (molarity) range from 8 to 16 M. They observed that with the increment of the molarity of the geopolymer mixture compressive strength was increased. Also, sodium silicate (Na_2SiO_3) is a high viscosity solution that is generally used with sodium hydroxide (NaOH) to enhance the compressive strength of FA-GPC; Na_2SiO_3 helps the formation of geopolymer gels and gives a high compact microstructure to the final product of the FA-GPC [26]. Furthermore, a variety of (Na_2SiO_3/NaOH) ratio was used to prepare geopolymer concrete, for instance, a research study has been carried out by Topark-Ngarm et al., [27], who used a different ratio of Na_2SiO_3/NaOH, and they reported that with the increasing of Na_2SiO_3/NaOH, compressive strength was increased. In the same context, the amount of aggregate content in the geopolymer mixture proportions have influences on the compressive strength of the FA-GPC as investigated by Joseph and Mathew [28]. They performed an experimental laboratory work that used different aggregate volumes from 60% to 75%., and they concluded that the FA-GPC with the total aggregate content of 70%, the ratio of sand to the total aggregate of 0.35, the molarity of 10, *l/b* of 0.55, Na_2SiO_3/NaOH of 2.5, when cured for 1 day at 100˚C, provide the compressive strength of 52 MPa.

Another critical parameter that affects the performance of FA-GPC is the curing condition of the samples. Generally, there are various types of curing regimes, namely, ambient curing [29,30], heat curing [31,32], and steam curing [33–35]. Several types of research have been carried out on the mixed proportion of FA-GPC and its compressive strength when cured at temperatures varying from 23 to 120˚C. The polymerization process is rapidly increased with the increment of curing temperature which makes the GC gain up to 70% of its final strength when the specimens cured inside an oven at 65˚C for 24 hr. beyond which there is a peripheral enhance in the compressive strength after 28 days of maturity [36,37]. Further, heat curing regimes give higher compressive strength as compared to the ambient curing condition for the

same GC mixture [38–41]. Experimental program work was done by Joseph and Mathew [28]. They used different curing temperatures from 30 to 100˚C to cure their GC specimens; their results show that with the increment of curing temperature, the compressive strength was significantly increased. Similar results were obtained by Chithambaram et al. [42].

Achieving an authoritative model for predicting the compressive strength of GC is essential regarding saving in time, energy, and cost-effectiveness. It gives guidance about scheduling for the construction process and removal of framework elements [43]. The modeling of the compressive strength characteristic of the FA-GPC is essential regarding the possibility of changing or validating the GC mix proportions [44]. By selecting appropriate mixing proportions, economical and efficient designs will be accomplished. Therefore, a variety of researches have been tried to shorten the time of selecting an appropriate mix of proportions to get the targeted properties; among them is modeling with developing empirical equations. There are different ways for modeling the characteristics of construction materials, including statistical techniques, computational modeling, and nowadays developed techniques such as regression analysis [45,46]. A variety of factors affect the compressive strength of the FA-GPC; this leads to different compressive strength results; as a consequence, predicting compressive strength is a challenging task for researchers and engineers. Therefore, there is a need for numerical and mathematical models [47]. Machine learning's excellent ability regarding prioritization, optimization, forecasting, and planning was widely used in the various engineering fields [43]. In the literature, machine learning systems were used to model the various characteristics of different types of concrete composites such as compressive strength of green concrete [48], splitting tensile and flexural strength of recycled aggregate concrete [49], modulus of elasticity of recycled concrete aggregate [50,51], the compressive strength of high volume fly ash concrete [52], the compressive strength of eco-friendly GC containing natural zeolite and silica fume [53], splitting tensile strength of fiber-reinforced concrete [54], and so on.

In the literature, there is a lack of measuring effects of several mixture proportion parameters and different curing regimes on the compressive strength of FA-GPC from an early age to 112 days. Also, according to the comprehensive and systematic review on the FA-GPC, an authoritative and developed model which used a variety of parameters to predict the compressive strength of FA-GPC is very rare to be used by the construction industry. The majority of efforts have concerned a single scale model without covering broad laboratory work data or various parameters. Moreover, the compressive strength of FA-GPC is affected by more than one parameter; therefore, in this study, for the first time, in a single developed model, influences of twelve parameters, such as SiO_2/Al_2O_3 (*Si/Al*) of fly ash, alkaline liquid/binder (*l/b*), fly ash (*FA*) content, fine aggregate (*F*) content, coarse aggregate (*C*) content, sodium hydroxide (*SH*) content, sodium silicate (*SS*) content, (*SS/SH*) ratio, molarity (*M*), curing temperature (*T*), curing duration inside ovens (*CD*) and specimens ages (*A*) were investigated and quantified on the compressive strength of FA-GPC by using different model techniques, namely Linear Regression (LR), Nonlinear regression (NLR) and Multi-logistic Regression (MLR). They were used as predictive models for predicting the compressive strength of eco-efficient FA-GPC by using 510 samples from the literature studies.

2. Research significance

Provide multiscale models to predict the compressive strength of FA-GPC is the main scope of this study. Thus, a wide range of laboratory work data, about 510 tested specimens with various (Si/Al), (l/b), (FA), (F), (C), (SH), (SS), (SS/SH), (M), (T), (CD), and (A) were considered with different analysis approaches aiming: (i) to guarantee the construction industry to use the provided models without any theoretical; (ii) to carry out statistical analysis and recognize the

influence of various parameters on the compressive strength of FA-GPC; (iii) to quantify and provide a systematic multiscale model to predict the compressive strength of FA-GPC with the mixture propositions containing a various range of parameters; (iv) to discover the most authoritative model to predict the compressive strength of FA-GPC from three different model techniques (LR, NLR, and MLR) using statistical assessment tools.

3. Methodology

510 dataset was collected from past researches on FA-GPC. In the literature, there is a wide range of data regarding geopolymer concrete with different base source materials, including FA, GGBFS, RHA, silica fume (SF), Metakaolin (MK), red mud (RM), and so on. But in this paper, the authors take those papers that use fly ash (FA) as base source materials to prepare geopolymer concrete. The models used twelve input parameters to restrict authors from using more datasets in the developed models. The collected datasets were statistically analyzed and split into three groups. The larger group, which included 340 datasets, was used to create the models. The second group consists of 85 datasets used to test the proposed models, and the last group, which includes 85 datasets, was used to validate the provided models [43]. The dataset ranges can be seen in Table 1 that contains the range of all different parameters with the measured compressive strength of FA-GPC. The input dataset consists of the Si/Al range from 0.4–7.7, l/b range from 0.25–0.92, FA range from 254–670 kg/m^3, F range from 318–1196 kg/m^3, C range from 394–1591 kg/m^3, SH range from 25–135 kg/m^3, SS range from 48–342 kg/m^3, SS/SH range from 0.4–8.8, M range from 3–20, T range from 23–120˚C, CD range from 8–168 hr, and A range from 3–112 days. The former dataset was then used to propose different models to predict the compressive strength of FA-GPC, and compared with the actual experimental compressive strength (MPa); after that, the developed models were assessed by some statistical criteria such as coefficient of determination, root mean squared error, mean absolute error, scatter index and OBJ to indicate the most reliable and accurate model. Further details of the data collection and modeling work are summarized in the form of a flow chart, as depicted in Fig 1.

4. Statistical assessment

In the current section, a statistical analysis was carried out to see whether powerful relationships exist between input parameters and compressive strength of FA-GPC or not. In this regard, all considered dataset variables including (1) SiO_2/Al_2O_3 (*Si/Al*) of fly ash (2), alkaline liquid/binder (*l/b*) (3), fly ash content (*FA*) (4), fine aggregate content (*F*) (5), coarse aggregate content (*C*) (6), sodium hydroxide (*SH*) (7), sodium silicate (*SS*) (8), (*SS/SH*) ratio (9), molarity (*M*) (10), curing temperature (*T*) (11), curing duration inside ovens (*CD*) (12), specimens ages (*A*) was plotted and analyzed with compressive strength, also, the statistical criteria such as standard deviation, variance, skewness, and kurtosis were determined to illustrate the distribution of each variable with compressive strength. Regarding the kurtosis criteria, a high negative value demonstrates the shorter distribution tails compared to the normal distribution, while the longer tails represent the positive value. A high negative value indicates a long left tail for the skewness parameter, and a positive value represents a right tail. More information on each statistical criterion was reported by Sliva et al. [96]. Below sufficient information regarding each variable considered as the input parameter is present:

a) SiO_2/Al_2O_3 (Si/Al)

Based on the dataset, which contains 510 data samples from literature, the Si/Al ratio of the fly ash was varied from 0.4 to 7.7 with an average of 2.7, the variance of 2.69, the standard deviation of 1.64, skewness of 2.5, and kurtosis of 5.03. Skewness belongs to distortion or asymmetry

Table 1. Summary of different fly ash-based geopolymer concrete mixes.

Ref.	(*Si/Al*)	(*l/b*)	*FA* (kg/m^3)	*F* (kg/m^3)	*C* (kg/m^3)	*SH* (kg/m^3)	*SS* (kg/m^3)	(*SS/SH*)	M	T (˚C)	CD (hr.)	A (Day)	*σc* (Mpa)
[21]	2	0.35	476	554	1294	48–120	48–120	0.4–2.5	8–14	24–90	8–96	3–94	17–64
[22]	4.3	0.35	334	555–632	1175–1329	58	58	1	13	90	8	7	17–61
[23]	2.2	0.3–0.45	400	830–895	830–895	32–52	85–129	2–3.3	12–18	50	48	7–28	16.36
[25]	2.1	0.45	350–400	505–533	1178–1243	45–52	112–129	2.5	8–16	24	-	3–28	7–41
[27]	2.2	0.5	414	588	1091	69–104	104–138	1–2	10–20	24–60	24	7–28	19–54
[28]	2.1	0.35–0.65	254–420	318–1198	394–1591	25–76	69–165	1.5–3.5	8–16	24–120	6–72	3–28	13–60
[29]	2.0	0.4	400	644	1197	53	107	2	10	24	-	3–56	5–23
[30]	1.8	0.4	394	554	1293	45	112	2.5	8	24	-	7–28	3–18
[31]	2.6	0.65	639	639	959	121	304	2.5	8_12	24	-	7–28	6–32
[32]	3.1	0.5	400	650	1206	50–70	140–154	2–2.75	14	60	168	7–28	30–36
[33]	1.6	0.35	408	647	1202	41	103	2.5	14	24–60	24	28	27–40
[34]	1.9	0.35	408	554	1294	41	103	2.5	8–14	60	24	7	40–64
[35]	1.9	0.35	356–444	554–647	1170–1248	36–44	89–111	2.5	14	60	24	7–28	24–63
[38]	2.1	0.38–0.46	350–400	540–575	1265–1343	38–53	95–132	2.5	16	24–90	24	3–28	2.6–44
[39]	0.4	0.4	350	650	1250	41	103	2.5	8	24–60	24	3–28	6–32
[40]	1.5	0.37	424	598	1169–1197	63	95	1.5	14	70	24	3–96	2–58
[41]	1.9	0.3	670	600	970	80	120	1.5	3–9	50	72	3–7	59–61
[42]	2.4	0.45	298–430	533–590	1243–1377	38–55	96–138	2.5	8–14	10–90	24	3–28	19–43
[55]	1.5–5.1	0.5–0.6	300–500	471–664	1000–1411	42–120	90–215	1.5–2	12–16	70	24	7	16–64
[56]	2.4	0.6	385	601.7	1203	66	165	2.5	12	80	24	3–28	74–81
[57]	1.8	0.45–0.55	300–350	698–753	1048–1131	38–55	96–118	2.5	10	100	24	7–28	26–36
[58]	3.0	0.81	409	686	909	129	204	1.58	15	80	24	28–96	22–27
[59]	2.3	0.4	394	646	1201	45	112	2.5	16	24–60	24	3–28	8–50
[60]	2.6	0.6	400	704	1056	68	171	2.5	10–16	60	24	7–28	25–32
[61]	1.5	0.35	408	554	1294	41	103	2.5	8	24	-	7–28	12–16
[62]	1.5	0.3–0.5	400–475	529–547	1235–1280	34–57	85–142	2.5	14	24	-	7–56	7–44
[63]	1.6	0.6	390	585	1092	67	167	2.5	8–18	24	-	28	23–32
[64]	2.1	0.35–0.38	408	660	1168–1201	41	103	2.5	10–16	24–50	24	28	25–72
[65]	2.8	0.55	356	554.4	1293	43–78	117–152	1.5–3.5	10	60	48	7–28	23–35
[66]	2.4–2.9	0.45	500	575	1150	64	160	2.5	14	24	-	28	44–52
[67]	2.4	0.4	440	723	1085	64	112	1.75	12	60	48	3–28	23–35
[68]	1.9	0.35	408	640–647	1190–1202	41	103	2.5	14–16	60	24	28	42–62
[69]	1.5–3.9	0.7–0.9	412–420	693–706	918–936	39–92	241–342	2.6–8.8	15	80	24	3–96	22–57
[70]	2.5	0.55	310	649	1204	48.86	122	2.5	10	80	24	28–96	44–47
[71]	1.9	0.4	400	651	1209	45	114	2.5	14	24	-	3–96	5–33
[72]	1.9	0.6	450	500	1150	135	135	1	10	40	24	7–96	18–49
[73]	1.7	0.4	400	554	1293	45	113	2.5	14	100	72	3–28	29–45
[74]	1.7	0.4	400	554	1293	45	113	2.5	14	100	72	3–28	29–45
[75]	1.9	0.37–0.4	408	647	1201	62–68	93–103	1.5	14	60	24	28	32–38
[76]	2.3–3.3	0.4	420–440	340–575	660–1127	60–68	150–169	2.5	12	80–120	72	7	21–61
[77]	3	0.35	409	549	1290	41	102	2.5	10	24	-	7–112	10–41
[78]	2.6–2.9	0.5	420	630	1090	60	150	2.5	12	80	24	7	32–41
[79]	2.3	0.5	368	554	1293	52	131	2.5	16	100	24	28	41
[80]	2.1–2.6	0.3	450	788–972	945–972	67	67	1	10	70	24	7–28	25–41
[81]	5.6	0.4	410	530	1044	67	117	1.74	10	24–75	26	7–180	4–36
[82]	2.3	0.45	500	550	1100	64.3	160.7	2.5	14	70	48	28	49.5
[83]	1.9	0.4	400	651–656	1209–1218	40–46	100–114	2.5	14	24	_	28–90	25–41

(*Continued*)

Table 1. (Continued)

Ref.	(*Si/Al*)	(*l/b*)	*FA* (kg/m^3)	*F* (kg/m^3)	*C* (kg/m^3)	*SH* (kg/m^3)	*SS* (kg/m^3)	(*SS/SH*)	M	T (˚C)	CD (hr.)	A (Day)	*σc* (Mpa)
[84]	1.7	0.4	400	554	1293	45	113	2.5	14	100	72	3–28	14–36
[85]	2.3	0.35–0.5	327–409	554–672	1201–1294	40–54	108–112	2–2.5	8–16	60	24	28	31–62
[86]	1.6	0.58	380	462	1386	62	156	2.5	10	60	24	28–56	18–23
[87]	1.9	0.4	394	554	1293	45	112	2.5	12	24–60	24	7–28	8–28
[88]	2.1	0.3–0.4	428	630	1170	44–57	114–122	2–2.5	8–14	60–90	24	3–7	20–49
[89]	1.5	0.3	563	732	5994	44	124	2.8	10	75	16	28	3345
[90]	7.7	0.4–0.6	345–394	554	1294	45–83	94–148	1.5–2.5	8–16	24	-	28	7–22
[91]	1.8	0.4	350	483	1081	40	100	2.5	14	24	-	7–28	3–23
[92]	1.7	0.45	436	654	1308	56	140	2.5	8	24	-	3–12	8–18
[93]	2.7	0.45	380	660	1189	48	122	2.5	8	24	-	28	30
[94]	1.6	0.35	500	623	1016	70	105	1.5	14–16	24	-	3–28	7–27
[95]	2.1	0.41	350	645	1200	41	103	2.5	8	24	-	3–56	7–21
Remarks (Ranged are Varies Between)	**0.4–7.7**	**0.25–0.92**	**254–670**	**318–1196**	**394–1591**	**25–135**	**48–342**	**0.4–8.8**	**3–20**	**23–120**	**8–168**	**3–112**	**2–64**

*(***Si/Al***) is a (SiO_2/Al_2O_3) ratio of fly ash, (***l/b***) is the alkaline liquid to binder ratio, (***FA***) is a fly ash content (kg/m^3), (***F***) is a fine aggregate content (kg/m^3), (***C***) is a coarse aggregate content (kg/m^3), (***SH***) is a sodium hydroxide content (kg/m^3), (***SS***) is a sodium silicate content (kg/m^3), (***SS/SH***) is the ratio of sodium silicate to sodium hydroxide of the mix, (***M***) is the molarity (concentration of sodium hydroxide) of the mix, (***T***) is the curing temperature of the specimens and this is may be ambient curing or heat curing inside an oven (˚C), (***CD***) is the curing duration inside an oven (hr.), (***A***) is the age of samples at the time of testing (days) and (***σc***) is the measured compressive strength (MPa).

https://doi.org/10.1371/journal.pone.0253006.t001

in a symmetrical normal distribution in a dataset. If the curve is moved to the right or the left side, it is stated to be skewed. Also, skewness could be quantified as an impersonation of the range to which a given distribution differs from a normal distribution. For instance, the skew of zero value was measured for normal distribution, while, right skew is an indication of log-normal distribution [97]. The variation between compressive strength and Si/Al, as well as the histogram analysis, is shown in Fig 2. As can be seen from figure a very poor relationship existed between compressive strength and the Si/Al ratio.

b) Alkaline liquid/binder (l/b)

According to the dataset, which contains 510 data samples from past researches, the l/b ratio of the FBGC was varied from 0.25 to 0.92 with an average variance, standard deviation, skewness, and kurtosis of 0.5, 0.01, 0.1, 1.21, and 2.88, respectively, The variance informed of the degree of spread in dataset, the greater the spread of the data, the greater the variance is about the mean. The relationship between compressive strength and l/b with Histogram of FA-GPC mixtures is presented in Fig 3.

c) Fly ash content (*FA*)

The content of fly ash in the mixture proportions of different FA-GPC for the collected data varied from 254 to 670 kg/m^3. The FAs have different chemical compositions as well as various specific gravities ranging from 1.95 to 2.54. The average, standard deviation, variance, skewness, and kurtosis of the FA were 386 kg/m^3, 63 kg/m^3, 3974, 1.51, and 6.18. The kurtosis is a statistical indicator that explains how heavily the tails of a distribution of a set of data differ from the tails of the normal distribution. In addition, the kurtosis finds the heaviness of the distribution tails, while skewness measures the symmetry of the distribution. Moreover, the

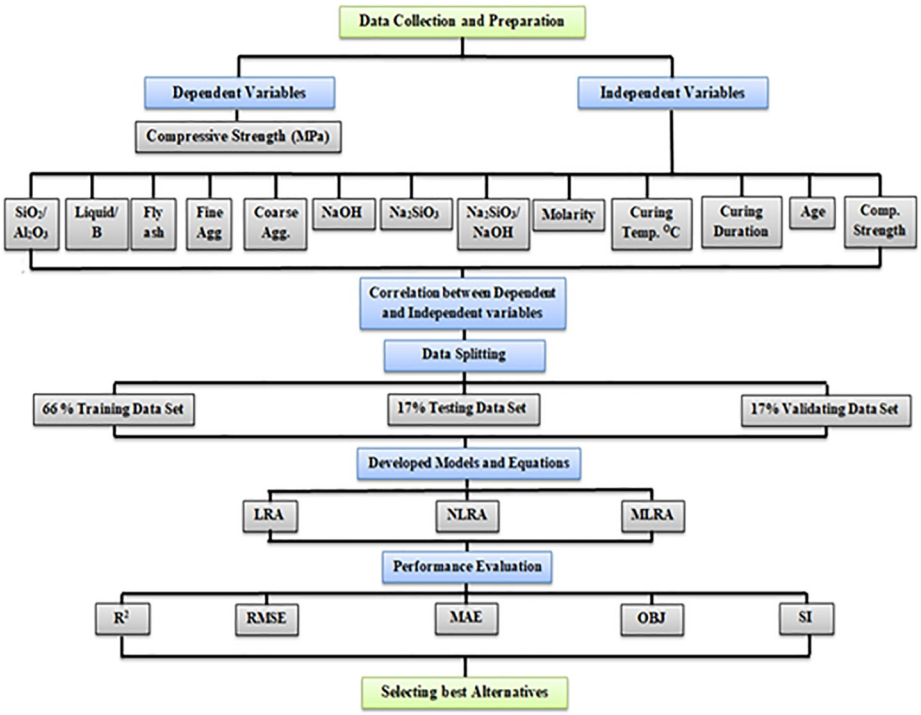

Fig 1. The flow chart diagram process followed in this study.

https://doi.org/10.1371/journal.pone.0253006.g001

variation between compressive strength and FA content and Histogram of FA-GPC mixtures is reported in Fig 4.

d) Fine aggregate content (*F*)

In the past studies, the fine aggregate was a river and crushed sand with a maximum aggregate size of 4.75 mm, and specific gravity ranged between 2.60–2.75. Also, its gradation satisfied the limitations of ASTM C 33. Fine aggregate content for the collected 510 datasets was varying from 318 to 1196 kg/m^3 for the mixtures of FA-GPC, and it has an average of 615kg/m^3, a standard deviation of 100 kg/m^3, a variance of 10047. Other statistical variables for the fine aggregate content in the FA-GPC mixtures, such as skewness and kurtosis, are 1.75 and 5.56. The relationship between compressive strength and fine aggregate content with a Histogram of FA-GPC mixtures is illustrated in Fig 5.

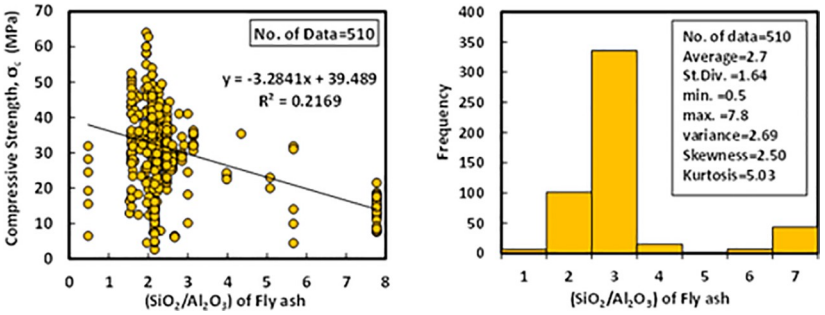

Fig 2. Variation between compressive strength and (SiO_2/Al_2O_3) ratio of fly ash with the histogram of fly ash-based geopolymer concrete mixtures.

https://doi.org/10.1371/journal.pone.0253006.g002

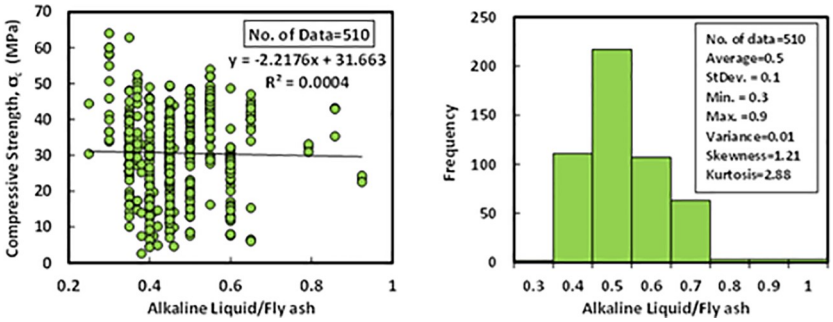

Fig 3. Variation between compressive strength and (alkaline liquid/fly ash) ratio with a histogram of fly ash-based geopolymer concrete mixtures.

https://doi.org/10.1371/journal.pone.0253006.g003

e) Coarse aggregate content (*C*)

The crushed stone or gravel with a maximum aggregate size of 20 mm was used in the literature as coarse aggregate for the production of FA-GPC. Based on the collected 510 dataset from different FA-GPC mixture proportions, coarse aggregate content varied between 394 to 1591 kg/m^3. The statistical analysis of the dataset shows that the average of the coarse aggregate content was 1187 kg/m^3, the standard deviation was 146.8 kg/m^3, the variance was 21557, the skewness was -1.69, and the kurtosis was 4.5. Variation between compressive strength and coarse aggregate content with Histogram of FA-GPC mixtures are presented in Fig 6.

f) Sodium hydroxide (*SH*)

The content of the sodium hydroxide (NaOH) for the collected 510 datasets varied from 25 to 135 kg/m^3, with an average of 54.3 kg/m^3, the standard deviation of 16.11 kg/m^3, and a variance of 259. The skewness and kurtosis were 1.69 and 4.55, respectively. The purity of the SH was above 97% of all the FA-GPC mixtures, and pellets and flakes were the two main states of the SH in all the mixtures. The relationship between compressive strength and sodium hydroxide with a Histogram of FA-GPC mixtures are illustrated in Fig 7.

g) Sodium silicate (*SS*)

Based on the dataset, which contains 510 data samples from literature, the content of SS was varied between 48 to 342 kg/m^3. The constituents of the SS were SiO_2, Na_2O, and water. The range of SiO_2 was varying from 28 to 37%, Na_2O was in the range of 8 to 18%, and the percent of water in the SS was in the range of 45 to 64%. The statistical analysis for the collected data of

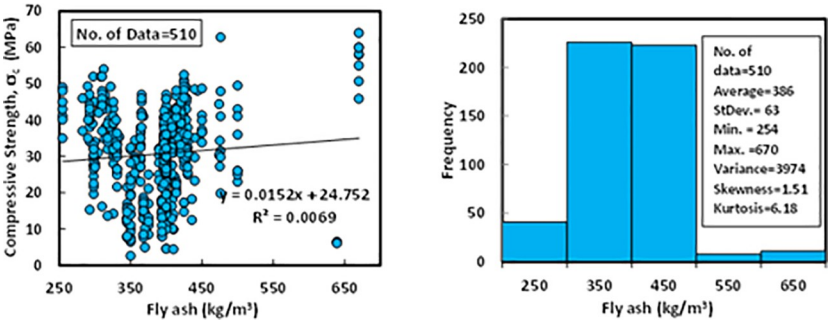

Fig 4. Variation between compressive strength and fly ash content with a histogram of fly ash-based geopolymer concrete mixtures.

https://doi.org/10.1371/journal.pone.0253006.g004

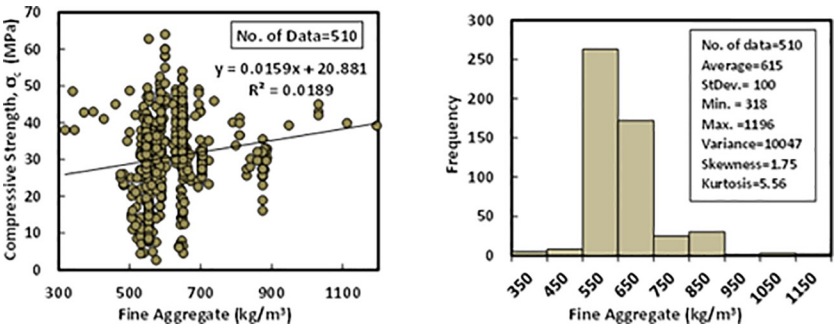

Fig 5. Variation between compressive strength and fine aggregate content with the histogram of fly ash-based geopolymer concrete mixtures.

https://doi.org/10.1371/journal.pone.0253006.g005

SS revealed that the average content of SS in the FA-GPC was 123.4 kg/m^3, the standard deviation was 36.2 kg/m^3, the variance was 1313, skewness was 2.89, and kurtosis was 12.8. Variation between compressive strength and sodium silicate (Na_2SiO_3) content with Histogram of FA-GPC mixtures are presented in Fig 8.

h) *SS/SH*

Referring to the collected data, the ratio of Na_2SiO_3 to NaOH was varied from 0.4 to 8.8, with an average of 2.4. The standard deviation, variance, skewness, and kurtosis were 0.68, 0.47, 4.71, and 45.9, respectively. The relationship between compressive strength and SS/SH with Histogram of FA-GPC mixtures is shown in Fig 9.

i) Molarity (*M*)

According to the dataset, which contains 510 data samples from literature, the sodium hydroxide concentration (molarity) was varying from 3 to 20 M, with an average of 11.9 M, the standard deviation of 2.8 M, the variance of 7.83, the skewness of 0.14 and the kurtosis of -0.41. Variation between compressive strength and molarity with Histogram of FA-GPC mixtures are illustrated in Fig 10.

j) Curing temperature (T)

The statistical analysis for the total collected data of the 510 dataset shows that the range of the curing temperature was varied from 23 to 120˚C, with an average of 58.6˚C and standard

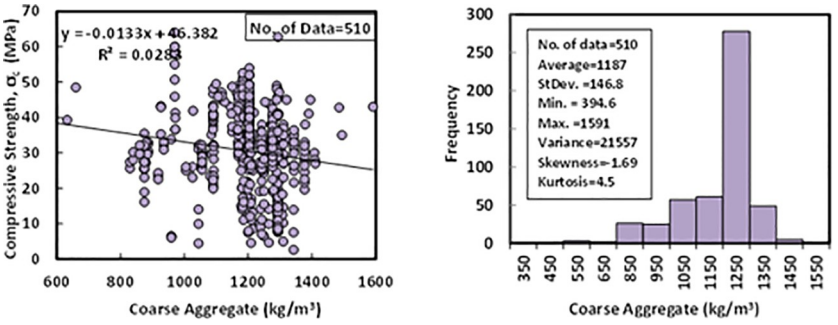

Fig 6. Variation between compressive strength and coarse aggregate content with a histogram of fly ash-based geopolymer concrete mixtures.

https://doi.org/10.1371/journal.pone.0253006.g006

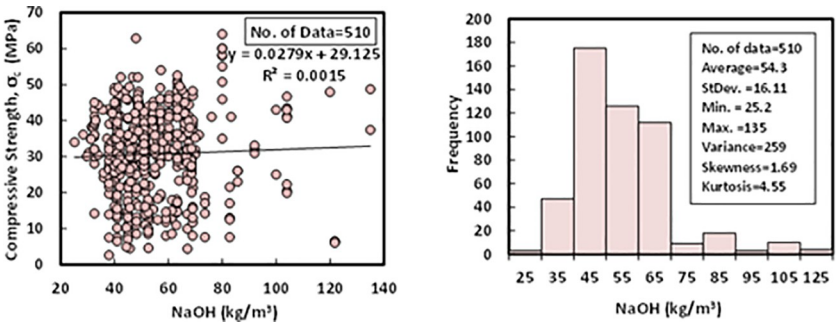

Fig 7. Variation between compressive strength and sodium hydroxide content with a histogram of fly ash-based geopolymer concrete mixtures.

https://doi.org/10.1371/journal.pone.0253006.g007

deviations of 27.9˚C. Besides, the variance, skewness, and kurtosis were 7, 0.05, and -1.16, correspondingly. The relationship between compressive strength and curing temperature with a Histogram of FA-GPC mixtures is shown in Fig 11.

k) Oven curing duration (*CD*)

The duration of heating samples in the oven with the selected temperatures was another independent variable that is collected from the past different research studies. The statistical analysis revealed that the minimum curing duration of the collected data set was 8 hr. The maximum CD inside ovens was 168 hr. Moreover, the average of CD was measured as 29 hr. the other statistical indications such as standard deviation, variance, skewness, and kurtosis were recorded as 19.86 hr, 395, 5.66, and 35.6, respectively. Variation between compressive strength and the oven curing duration with Histogram of FA-GPC mixtures are illustrated in Fig 12.

l) Specimens ages (*A*)

Another independent variable collected in the literature papers is the age of FA-GPC specimens. The collected data contain the ages of the samples range from 3 up to 112 days. Other statistical measuring devices such as standard deviation, variance, skewness, and kurtosis were calculated as 15.65 days, 245, 2.67, and 10.75, correspondingly. Variation between compressive strength and specimens ages with Histogram of FA-GPC mixtures are shown in Fig 13.

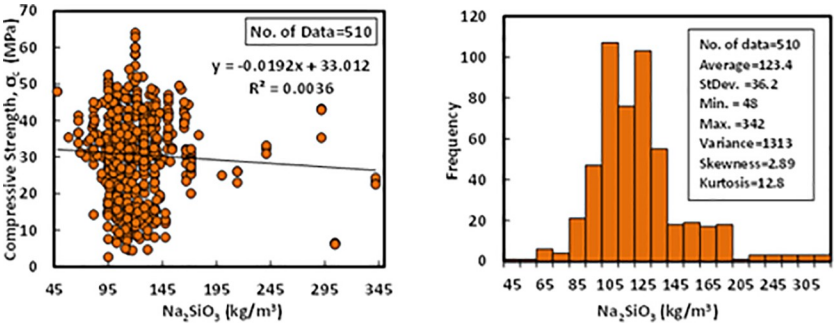

Fig 8. Variation between compressive strength and sodium silicate content with histogram of fly ash-based geopolymer concrete mixtures.

https://doi.org/10.1371/journal.pone.0253006.g008

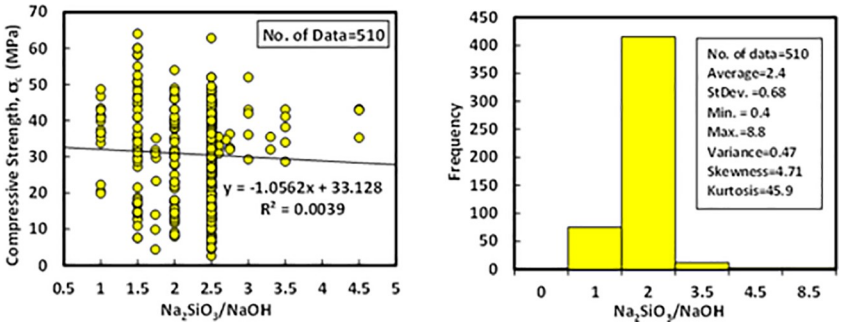

Fig 9. Variation between compressive strength and (SS/SH) ratio with a histogram of fly ash-based geopolymer concrete mixtures.

https://doi.org/10.1371/journal.pone.0253006.g009

m) Compressive strength (σc)

The measured compressive strength of the 510 collected data from the literature studies was shown in Table 1; the compressive strength of the FA-GPC was in the range of 2 to 64 MPa, with an average of 30.6 MPa. The statistical analysis for the other dataset distribution indications such as standard deviation, variance, skewness, and kurtosis was 11.6 MPa, 133.8, -0.16, and -0.3, respectively.

5. Modeling

Based on the coefficient of determination (R^2) and statistical analysis, there are no direct relationships between the compressive strength and the constituents of the FA-GPC at different curing regimes as shown in Figs 2–13. Therefore, three different models, as reported below, are proposed to evaluate the impact of different mixture proportions mentioned above on the compressive strength of FA-GPC.

The models proposed in this study are used to predict the compressive strength of FA-GPC and select the best model, which gives a better estimation of compressive strength compared with the measured compressive strength from the experimental data. All the collected datasets were randomly split in to three parts, namely training, testing, and validating datasets [43]. 340 Training dataset is used to train the LR, NLR, and MLR model and obtain the optimal weights and biases, while 85 testing dataset is used to confirm the fulfillment of the proposed models. Moreover, 85 validating datasets are used to explore the generality of the models and prohibition of the over-fitting problem in the case of classical training algorithms. The comparison

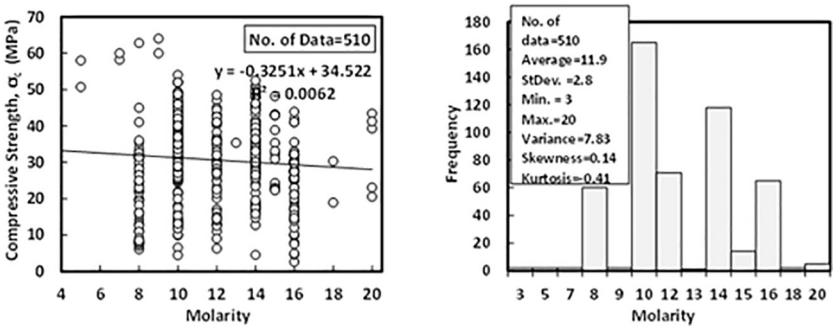

Fig 10. Variation between compressive strength and molarity with a histogram of fly ash-based geopolymer concrete mixtures.

https://doi.org/10.1371/journal.pone.0253006.g010

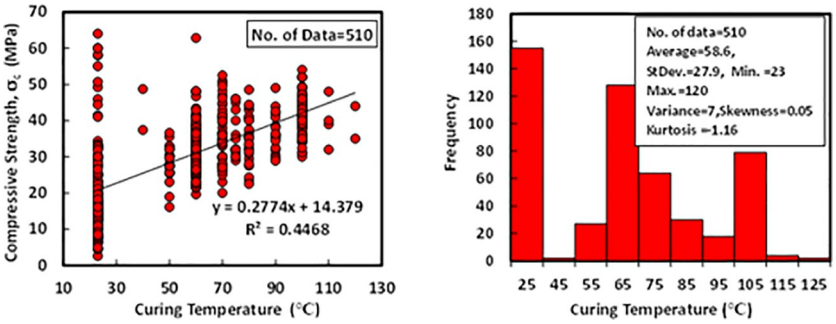

Fig 11. Variation between compressive strength and curing temperature histogram of fly ash-based geopolymer concrete mixtures.

https://doi.org/10.1371/journal.pone.0253006.g011

among model predictions was made based on the following assessment criteria: the model should be scientifically valid, it should give less percentage of error between the measured and predicted data, lower RMSE, OBJ, SI, and higher R^2 value.

a) Linear regression model (LR)

One of the most common methods to predict the compressive strength of concrete is the linear regression model (LR) [98], as shown in Eq 1, and it is considered as a general form of linear regression model [52,97]

$$\sigma c = a + b(l/b) \tag{1}$$

Where, σc, $^{l}/_{b}$, *a and b* represents compressive strength, liquid to binder ratio and equation parameters, respectively. However, other components of FA-GPC mixtures that influence the compression strength, such as curing regime and time and different mix proportions, are not included in the equation above. Therefore, to have more reliable and scientific observations, Eq 2 is proposed to include all other mix proportions and variables that may impact the compressive strength of FA-GPC.

$$\sigma c = a + b\left(\frac{Si}{Al}\right) + c\left(\frac{l}{b}\right) + d(FA) + e(F) + f(C) + g(SH) + h(SS) + i\left(\frac{SS}{SH}\right) + j(M) + k(A) + l(T) + m(CD) \tag{2}$$

Where: (Si/Al) is the ratio of SiO_2 to Al_2O_3 of the fly ash, (l/b) is the alkaline liquid to the

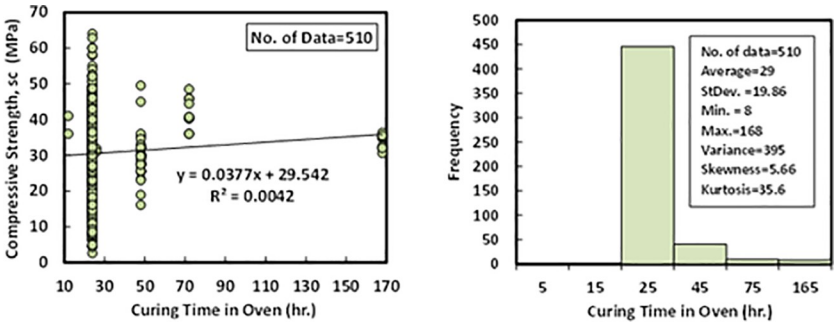

Fig 12. Variation between compressive strength and curing duration with histogram of fly ash-based geopolymer concrete mixtures.

https://doi.org/10.1371/journal.pone.0253006.g012

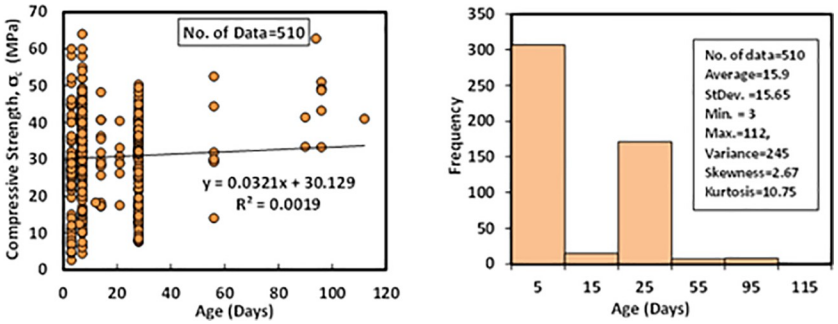

Fig 13. Variation between compressive strength and curing duration histogram of fly ash-based geopolymer concrete mixtures.

https://doi.org/10.1371/journal.pone.0253006.g013

binder ratio, (*FA*) is the fly ash content (kg/m^3), (*F*) is the fine aggregate content (kg/m^3), (*C*) is the coarse aggregate content (kg/m^3), (*SH*) is the sodium hydroxide content (kg/m^3), (*SS*) is the sodium silicate content (kg/m^3), (*SS/SH*) is the ratio of sodium silicate to the sodium hydroxide, (*M*) is the sodium hydroxide concentration (Molarity), (*T*) is the curing temperature (˚C), (*CD*) is the curing duration inside ovens (hr) and (*A*) is the ages of the specimens (days). While *a*, *b*, *c*, *d*, *e*, *f*, *g*, *h*, *i*, *j*, *k*, *l*, and *m* are the model parameters. This developed equation is a unique equation that involves a wide range of independent variables to produce FA-GPC that may be very useful for the construction industry. The proposed Eq 2 can be considered as an extent for Eq 1 since all variables can be adapted linearly.

b) Nonlinear regression model (NLR)

To propose a NLR model, Eq 3 could be considered as a general form [99,100]. The interrelation between different variables in Eqs 1 and 2 can be represented in Eq 3 to predict the compression strength of FA-GPC mixtures.

$$\sigma c = a * \left(\frac{Si}{Al}\right)^{b} * (\frac{l}{b})^{c} * (FA)^{d} * (F)^{e} * (C)^{f} * (SH)^{g} * (SS)^{h} * \left(\frac{SS}{SH}\right)^{i} * (M)^{j} * (A)^{k} + l * \left(\frac{Si}{Al}\right)^{m} * \left(\frac{l}{b}\right)^{n} * (FA)^{o} * (F)^{p} * (C)^{q} * (SH)^{r} * (SS)^{s} * \left(\frac{SS}{SH}\right)^{t} * (M)^{u} * (A)^{v} * (T)^{w} * (CD)^{x} \quad (3)$$

Where: (*Si/Al*) is the ratio of SiO_2 to Al_2O_3 of the fly ash, (*l/b*) is the alkaline liquid to the binder ratio, (*FA*) is the fly ash content (kg/m^3), (*F*) is the fine aggregate content (kg/m^3), (*C*) is the coarse aggregate content (kg/m^3), (*SH*) is the sodium hydroxide content (kg/m^3), (*SS*) is the sodium silicate content (kg/m^3), (*SS/SH*) is the ratio of sodium silicate to the sodium hydroxide, (*M*) is the sodium hydroxide concentration (Molarity), (*T*) is the curing temperature (˚C), (*CD*) is the curing duration inside ovens (hr.) and (*A*) is the ages of the specimens (Days). While, *a*, *b*, *c*, *d*, *e*, *f*, *g*, *h*, *i*, *j*, *k*, *l*, *m*, *n*, *o*, *p*, *q*, *r*, *s*, *t*, *u*, *v*, *w*, and *x* are the model parameters.

c) Multi-logistic regression model (MLR)

Same as the former models, multi-logistic regression analysis model was carried out for the collected datasets, and the general form of the MLR is shown in Eq 4 based on the research studied that had been conducted by Mohammed et al. [51]. MLR is used to clarify the

difference between a nominal predictor variable and one or more independent variables.

$$\sigma_c = a47208 een\ model\ predictions\ of\ compressive\ strength\ of\ fly\ ash\ based\ geopolymer\ concrete\ mixtures\ using\ training\ data 161616$$

$$* \left(\frac{Si}{Al}\right)^{b} * \left(\frac{l}{b}\right)^{c} * (FA)^{d} * (F)^{e} * (C)^{f} * (SH)^{g} * (SS)^{h} * \left(\frac{SS}{SH}\right)^{i} * (M)^{j} * (A)^{k} * (T)^{l} * (CD)^{m} \quad (4)$$

Where: (Si/Al) is the ratio of SiO_2 to Al_2O_3 of the fly ash, (l/b) is the alkaline liquid to the binder ratio, (FA) is the fly ash content (kg/m^3), (F) is the fine aggregate content (kg/m^3), (C) is the coarse aggregate content (kg/m^3), (SH) is the sodium hydroxide content (kg/m^3), (SS) is the sodium silicate content (kg/m^3), (SS/SH) is the ratio of sodium silicate to the sodium hydroxide, (M) is the sodium hydroxide concentration (Molarity), (T) is the curing temperature (˚C), (CD) is the curing duration inside ovens (hr.) and (A) is the ages of the specimens (Days). While a, b, c, d, e, f, g, h, i, j, k, l, and m are the model parameters.

6. Model performance assessment criteria

In order to evaluate and assess the efficiency of the proposed models, various performance parameters, including the coefficient of determination (R^2), Root Mean Squared Error (RMSE), Mean Absolute Error (MAE), Scatter Index (SI), and OBJ, were used, which are defined as follows:

$$R^2 = \left(\frac{\sum_{p=1}^{p} (t_p - t')(y_p - y')}{\sqrt{[\sum_{p=1}^{p} (t_p - t')^2][\sum_{p=1}^{p} (y_p - y')^2]}} \right)^2 \quad (5)$$

$$RMSE = \sqrt{\frac{\sum_{p=1}^{p} (y_p - t_p)^2}{p}} \quad (6)$$

$$MAE = \frac{\sum_{p=1}^{p} |(y_p - t_p)|}{p} \quad (7)$$

$$SI = \frac{RMSE}{t'} \quad (8)$$

$$OBJ = \left(\frac{n_{tr}}{n_{all}} * \frac{RMSE_{tr} + MAE_{tr}}{R^2_{tr} + 1}\right) + \left(\frac{n_{tst}}{n_{all}} * \frac{RMSE_{tst} + MAE_{tst}}{R^2_{tst} + 1}\right) + \left(\frac{n_{val}}{n_{all}} * \frac{RMSE_{val} + MAE_{val}}{R^2_{val} + 1}\right) \quad (9)$$

Where: $\boldsymbol{y_p}$ and $\boldsymbol{t_p}$ are the predicted and the measured values of the pth pattern, correspondingly, and $\boldsymbol{t'}$ and $\boldsymbol{y'}$ are the averages of the measured and the predicted values, respectively. ***tr***, ***tst,*** and ***val*** are referred to as training, testing, and validating datasets, respectively and ***n*** is the number of patterns (collected data) in the corresponding dataset.

Except for the R^2 value, the best value for other assessment parameters is zero. However, the best value for R^2 is one. Regarding the SI parameter, it can be said that a model has a poor performance when SI > 0.3, a fair performance when $0.2 <$ SI < 0.3, a good performance when $0.1 <$ SI < 0.2, and an excellent performance when SI < 0.1 [43,101]. Moreover, in Eq (9) the OBJ parameter was also used to assess the efficiency of the proposed models as an integrated performance parameter.

7. Analysis and outputs

a) LR model

The comparison between predicted and measured compressive strengths of FA-GPC for training, testing and validating datasets are presented in Fig 14A–14C, respectively. The model parameters observed that the l/b ratio and the ratio of sodium silicate to the sodium hydroxide significantly affects the compressive strength of FA-GPC. For the current model the weight of each parameter on the compressive strength of FA-GPC was determined by optimizing the sum of error squares and the least square method, which implemented in Excel program using Solver to calculate the ideal value (a specific value, minimum or maximum) for the equation in one cell named the objective cell. This object cell was subject to certain limits or constraints on the values of other equation cells in the worksheet [52]. Based on the linear regression analysis model, it was observed that, among the whole model input parameters, the ratio of alkaline liquid to the binder ration (*l*/*b*) and the sodium silicate to the sodium hydroxide ratio of the GC mixture have a great influence on the compressive strength of the FA-GPC which it is matched with the experimental results presented in the literature [21,23,25,28,55]. The equation for the LR model with different weight parameters can be written as follows as reported in Eq 10.

$$\sigma c = -66.8 - 1.697\left(\frac{Si}{Al}\right) + 187.75\left(\frac{l}{b}\right) + 0.246(FA) - 0.016(F) - 0.012(C) - 0.334(SH) - 0.538(SS) + 0.942\left(\frac{SS}{SH}\right) + 0.179(M) + 0.228(A) + 0.342(T) + 0.01(CD) \quad (10)$$

The studied datasets have a ±20% error line for the training data and -15% and +20% error lines for both testing and validating datasets. Nevertheless, the developed model slightly overestimated the low strength FA-GPC mixes and underestimated the high strength FA-GPC. Also, the residual compressive strength between the predicted and measured compressive strength for the LR model by using training, testing, and validating dataset were compared, as shown in Fig 15. This model's evaluation parameters, such as R^2, RMSE, and MAE are 0.8369, 4.65 MPa, and 3.76 MPa, respectively. Moreover, as reported from Figs 16 and 17, the OBJ and SI values for the current model are 3.09 and 0.15 for the training dataset.

b) NLR model

The relationships between the predicted compressive strength and measured compressive strength obtained from experimental programs of FA-GPC mixtures for training, testing, and

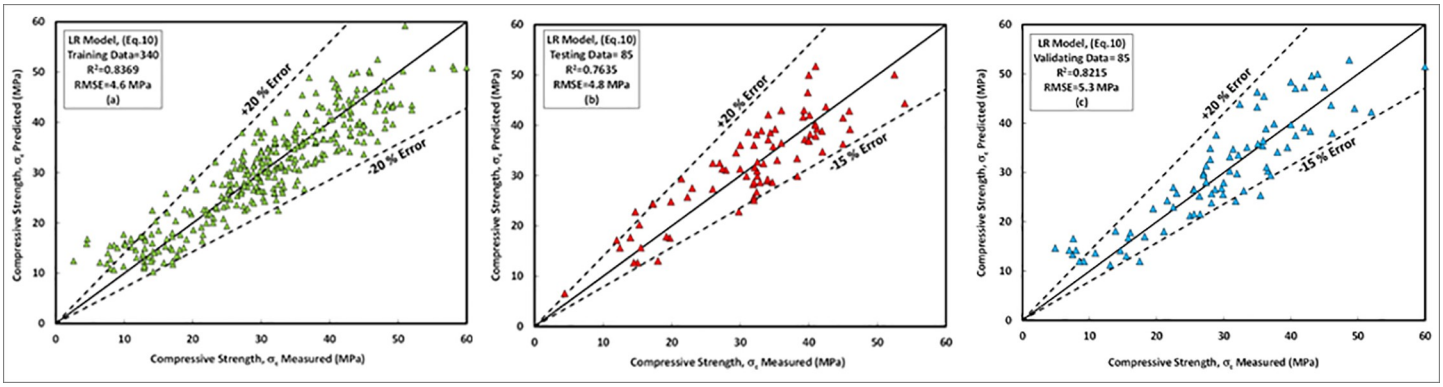

Fig 14. Comparison between measured and predicted compressive strength of fly ash-based geopolymer concrete mixture using LR model, (a) training data, (b) testing data, (c) validating data.

https://doi.org/10.1371/journal.pone.0253006.g014

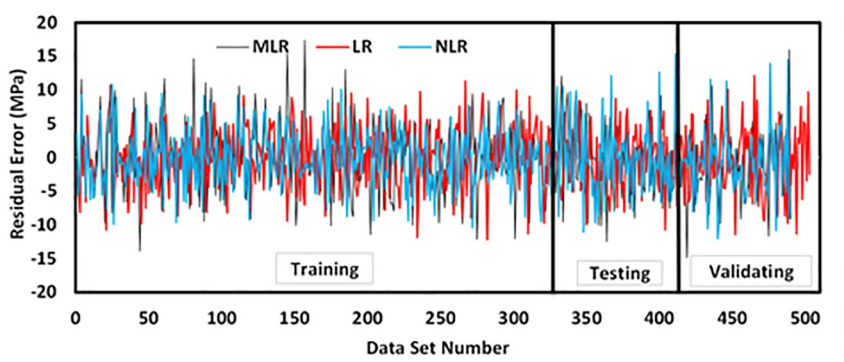

Fig 15. Residual error diagram of compressive strength of fly ash-based geopolymer concrete mixtures using training, testing, and validating dataset for all models.

https://doi.org/10.1371/journal.pone.0253006.g015

validating datasets are presented in Fig 18A–18C, respectively. The most important parameters which affects the compressive strength of FA-GPC mixtures according to this model are the curing temperature and sodium silicate content. This was also approved by several experimental programs from past studies, in which increasing the sodium silicate content and increasing the curing temperature was resulted in the increasing the compressive strength of FA-GPC mixtures significantly [21,27,31,38,40,55,81,87,92]—the proposed equation for NLR model with different variable parameters presented in Eq 11.

$$\sigma_C = -1997208 * \left(\frac{Si}{Al}\right)^{-0.508} * \left(\frac{l}{b}\right)^{-1.606} * (FA)^{-2.134} * (F)^{0.016} * (C)^{0.089} * (SH)^{-0.27} * (SS)^{0.274} * \left(\frac{SS}{SH}\right)^{-0.533} * (M)^{0.117} * (A)^{-0.305} + 9993.13 * \left(\frac{Si}{Al}\right)^{-0.423} * \left(\frac{l}{b}\right)^{-0.068} * (FA)^{-0.368} * (F)^{-0.151} * (C)^{-0.184} * (SH)^{-0.426} * (SS)^{-0.0007} * \left(\frac{SS}{SH}\right)^{-0.453} * (M)^{0.134} * (A)^{-0.022} * (T)^{0.352} * (CD)^{-0.064} \quad (11)$$

The studied datasets have a ±20% error line for the training data and -15% and +20% error lines for both testing and validating datasets. Similar to the LR model, this model slightly

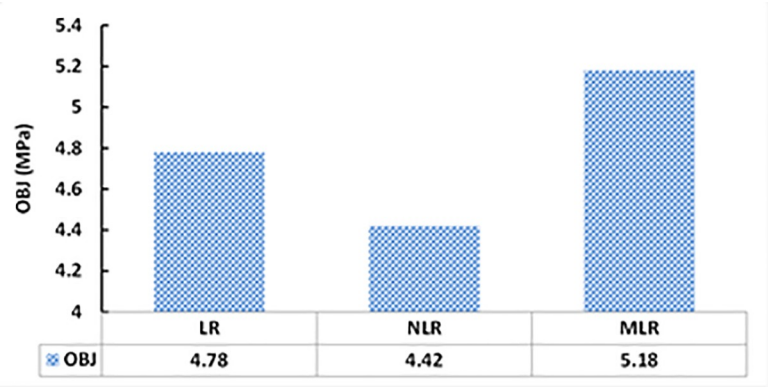

Fig 16. The OBJ values of all developed models.

https://doi.org/10.1371/journal.pone.0253006.g016

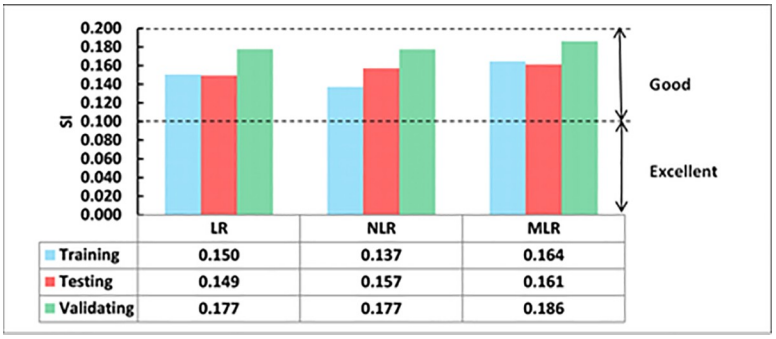

Fig 17. Comparing the SI performance parameter of different developed models.

https://doi.org/10.1371/journal.pone.0253006.g017

underestimated the high strength FA-GPC mixes and overestimated the low strength FA-GPC. Also, the residual compressive strength was shown in Fig 15, which shows the residual error between the predicted and measured compressive strength for the NLR model by using training, testing, and validating datasets. In addition, the assessment parameters for this model, such as R^2, RMSE, and MAE, are 0.8576, 4.19 MPa, and 3.35 MPa, respectively, and the other assessment tools such as OBJ and SI are 2.71 and 0.14 correspondingly, as illustrated from Figs 16 and 17.

c) MLR model

The proposed equation for MLR model with different variable parameters presented in Eq 12. In the MLR model, like other developed models, the curing temperature, sodium silicate content, an alkaline liquid to the binder ratio were the most significant independent variables that affect on the compressive strength of the FA-GPC that is matched with the experimental works presented in the literature [21,23,25,27,28,31,38,40,55,81,87,92]. The relationships between the predicted and measured compressive strength of the training data set for FA-GPC was shown in Fig 19A. Further, same as the two previous models, this model was checked by two sets of data (testing and validating dataset) to show their efficiency for other data out of the model data (training data); the results show that this model can be used to predict the compressive strength of FA-GPC just by substitute the independent variables into the developed

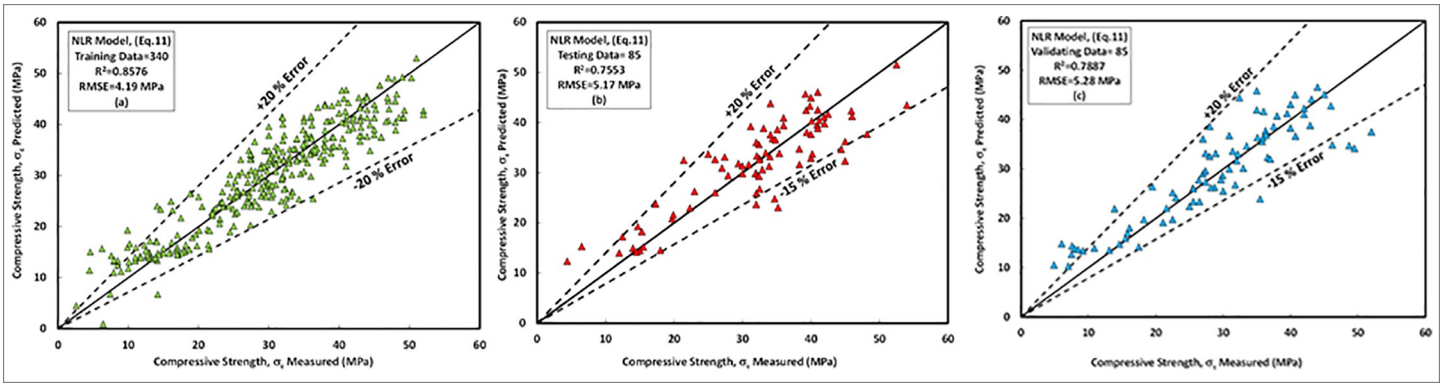

Fig 18. Comparison between measured and predicted compressive strength of fly ash-based geopolymer concrete mixture using NLR model, (a) training data, (b) testing data, (c) validating data.

https://doi.org/10.1371/journal.pone.0253006.g018

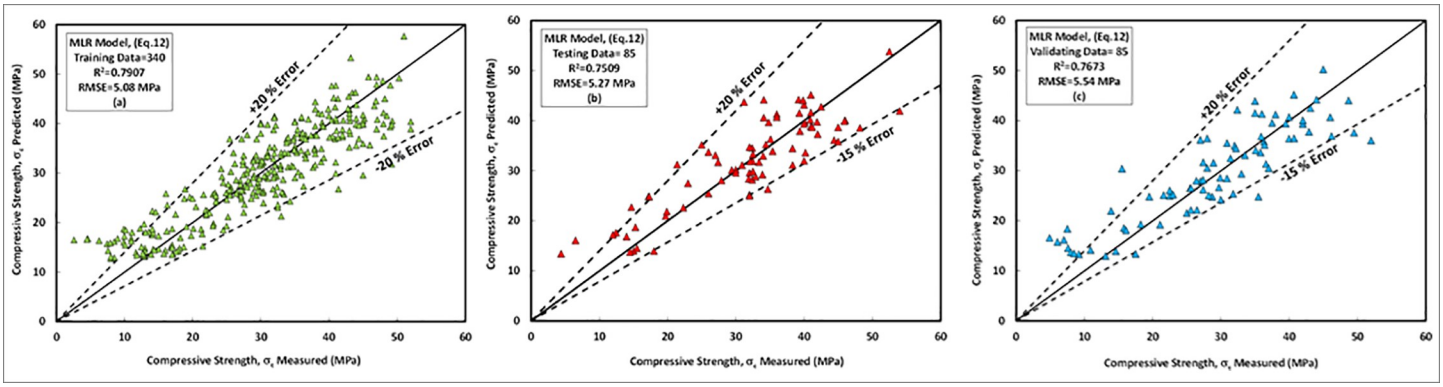

Fig 19. Comparison between measured and predicted compressive strength of fly ash-based geopolymer concrete mixture using MLR model, (a) training data, (b) testing data, (c) validating data.

https://doi.org/10.1371/journal.pone.0253006.g019

equation as shown in Fig 19B and 19C.

$$\sigma_c = 147.1447208 \textit{een model predictions of compressive strength of fly ash based geopolymer concrete mixtures using training data} 191919 * \left(\frac{Si}{Al}\right)^{-0.383} * \left(\frac{l}{b}\right)^{0.350} * (FA)^{0.195} * (F)^{-0.212} * (C)^{-0.236} * (SH)^{-0.715} * (SS)^{0.393} * \left(\frac{SS}{SH}\right)^{-0.81} * (M)^{0.086} * (A)^{0.128} * (T)^{0.534} * (CD)^{-0.046} \quad (12)$$

Similar to other models, the studied datasets have a ±20% error line for the training data and -15% and +20% error lines for both testing and validating datasets, which indicated that almost all checked results were in ± 20% error lines. Finally, the residual compressive strength for the MLRA model was shown in Fig 15 for the predicted and measured compressive strength using training, testing, and validating datasets. Furthermore, the assessment criteria for this model, such as R^2, RMSE, MAE, OBJ, and SI are 0.7907, 5.08 MPa, 3.95 MPa, 3.4, and 0.17, respectively, for the training dataset.

8. Comparison between developed models

As mentioned previously, five different statistical tools, which are RMSE, MAE, SI, OBJ, and R^2 was used to evaluate the efficiency of the developed models. Among the three different models, the NLR model has higher R^2 with lower RMSE and MAE values compared to LR and MLR models. Also, Fig 20 presents the comparison between model predictions of the compressive strength of FA-GPC mixtures using training data. Moreover, Fig 15 shows the residual error for all models using training, testing, and validating datasets. It can be noticed from both figures that the predicted and measured values of compressive strength are closer for the NLR mode, which indicates the superior performance of the NLR model compared to other models.

The OBJ values for all proposed models are given in Fig 16. The values for LR, NLR, and MLR are 4.78, 4.42, and 5.18, respectively. The OBJ value of the NLR model is 8.1% less than the LR model and 17.2% lower than the NLR models. This also demonstrates that the NLR model is more efficient for predicting the compressive strength of FA-GPC mixtures.

The values of the SI assessment parameter for the proposed models in the training, validating, and testing phases are presented in Fig 17. As can be seen from Fig 17, for all models and all phases (Training, testing, and validating), the SI values were between 0.1 and 0.2, indicating good performance for all models. However, similar to the other performance parameters the NLR model has lower SI values compared to other models. The NLR model has 9.4% and 19.7% lower SI values than LR and MLR models, correspondingly. This also illustrated that the

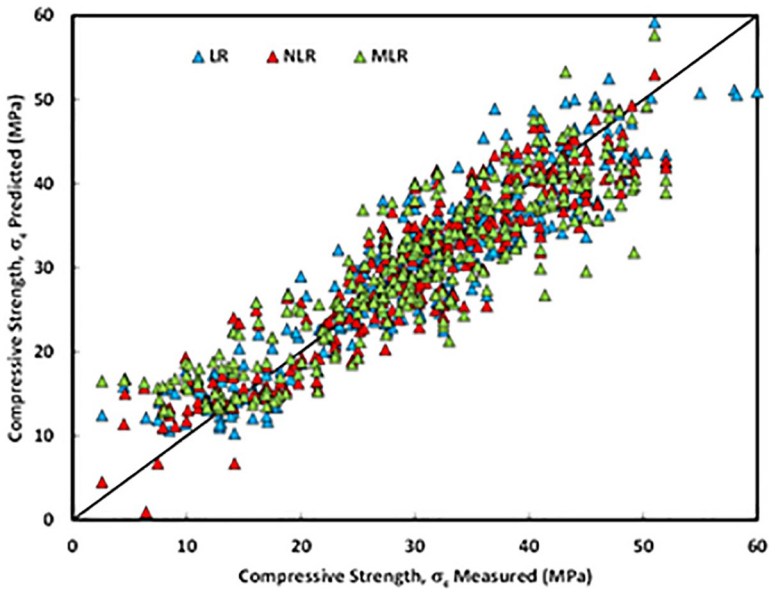

Fig 20. Compression between model predictions of compressive strength of fly ash-based geopolymer concrete mixtures using training data.

https://doi.org/10.1371/journal.pone.0253006.g020

NLR model is more efficient and performed better compared to LR and MLR models for predicting the compressive strength of FA-GPC.

9. Sensitivity investigation

In order to find and assess the essential input parameter that affects the compressive strength of FA-GPC, a sensitivity comparison was carried out for the whole model [97]. The training dataset for the models was calculated by Solver in Excel. During the sensitivity analysis, several different training data sets were used. For each set, a single input variable was extracted at a time, and the effects of this variable were assessed by R^2, RMSE, MAE, OBJ, and SI, which is illustrated in Table 2. According to the obtained results, the curing temperature is the most

Table 2. Sensitivity analysis using LRA, NLRA, and MLRA model.

		LR Model					NLR Model					MLR Model				
		R^2	RMSE	MAE	OBJ	SI	R2	RMSE	MAE	OBJ	SI	R2	RMSE	MAE	OBJ	SI
Removed Parameter	**None**	0.84	4.65	3.76	3.09	0.15	0.86	4.19	3.35	2.71	0.14	0.79	5.09	3.95	3.40	0.17
	Si/Al	0.71	6.20	4.96	4.41	0.20	0.78	5.23	4.11	3.51	0.18	0.71	6.02	4.79	4.27	0.20
	l/b	0.73	6.01	4.75	4.21	0.20	0.86	4.23	3.33	3.22	0.18	0.79	5.10	3.95	3.41	0.17
	***FA* (kg/m^3)**	0.69	6.43	4.90	4.54	0.21	0.86	4.22	3.34	2.72	0.14	0.79	5.09	3.94	3.40	0.17
	***F* (kg/m^3)**	0.83	4.73	3.84	3.17	0.16	0.85	4.25	3.37	2.75	0.14	0.79	5.13	3.97	3.43	0.17
	***C* (kg/m^3)**	0.79	5.24	4.15	3.54	0.17	0.85	4.27	3.37	2.75	0.14	0.79	5.13	3.96	3.43	0.17
	SH (kg/m^3)	0.79	5.27	4.21	3.58	0.17	0.85	4.24	3.37	2.75	0.14	0.79	5.11	3.97	3.42	0.17
	***SS* (kg/m^3)**	0.72	6.12	4.83	4.31	0.20	0.86	4.19	3.34	2.71	0.14	0.79	5.09	3.96	3.41	0.17
	SS/SH	0.84	4.65	3.78	3.10	0.15	0.86	4.20	3.36	2.72	0.14	0.79	5.12	3.98	3.43	0.17
	M	0.84	4.67	3.79	3.11	0.15	0.85	4.27	3.43	2.75	0.14	0.79	5.11	3.99	3.43	0.17
	***T* (˚C)**	**0.40**	**8.90**	**7.00**	**7.67**	**0.29**	**0.43**	**8.43**	**6.71**	**7.11**	**0.28**	**0.36**	**8.88**	**6.98**	**7.84**	**0.29**
	***CD* (hr.)**	0.84	4.65	3.76	3.09	0.15	0.85	4.26	3.39	2.76	0.14	0.79	5.10	3.95	3.41	0.17
	***A* (Day)**	0.75	5.70	4.47	3.92	0.19	0.76	5.40	4.23	3.65	0.18	0.71	6.01	4.67	4.21	0.20

https://doi.org/10.1371/journal.pone.0253006.t002

significant variable for the prediction of the compressive strength of FA-GPC for the whole LR, NLR, and MLR models, and this is match with a variety of researches that have been performed in the literature [21,27,31,40,81,87,92]. In this study, the curing temperature for the obtained data was ranged from 23 to 120˚C, thus increasing the curing temperature considerably increased the compressive strength of FA-GPC. It is well documented in the literature that the compressive strength of FA-GPC is significantly affected by the curing temperature and duration. Longer curing time and curing at high temperature (50–100˚C) increases the compressive strength of FA-GPC, although the increase in strength may be insignificant for curing at more than 60˚C and for periods longer than 48 hrs. Therefore, for heat curing regimes, temperatures between 50–80˚C and curing time of 24 hr are widely accepted values used for a successful polymerization process. In addition, among the curing condition methods (oven, steam, and ambient), oven curing techniques have a better influence on the compressive strength of FA-GPC composites.

10. Conclusions

Predicting of compressive strength of FA-GPC by the reliable and accurate model can save time and cost. In this paper, linear regression (LR), nonlinear regression (NLR), and multilogistic regression (MLR) were used to propose predictive models for the FBGC. Based on the 510 collected dataset from previous research works and the simulation of the compressive strength of the FA-GPC, the following conclusion can be drawn:

i. All the used models LR, NLR, and MLR could be successfully used to develop predictive models for the compressive strength of the FA-GPC. Overall, the NLR model has better performance than the other two models. The R^2 values for this model are 0.86, 0.75, and 0.79 for the training, testing, and validating datasets, respectively. In addition, other sensitivity indicators for the training dataset for the NLR model are 4.19 MPa, 3.35 MPa, 2.71, and 0.14 for the RMSE, MAE, OBJ, and SI, respectively.

ii. The R^2, RMSE, MAE, OBJ, and SI values were 0.84, 4.65MPa, 3.76MPa, 3.09, and 0.15, correspondingly, for the LR model for the training dataset. While these values are 0.79, 5.09 MPa, 3.95 MPa, 3.40, and 0.17, respectively, for the MLR model.

iii. The assessment and comparison of statistical parameters R^2, RMSE, MAE, OBJ, and SI for all the training, testing, and validating datasets validate the accuracy of the developed models properly.

iv. According to the sensitivity analysis approaches, the curing temperature, liquid to binder ratio, and sodium silicate content are the most effective independent variables for predicting the compressive strength of FA-GPC for all the models.

v. The eco-efficient fly ash-based geopolymer concrete studied here can participate in sustainable development because it is a cementless concrete and used industrial or agro by-product ashes as a binder material; these mixture properties lead to a reduction of the carbon dioxide percent in the air, energy consumption, as well as waste disposal and the cost of the construction.

Author Contributions

Conceptualization: Ahmed Salih Mohammed, Azad A. Mohammed.

Investigation: Hemn Unis Ahmed.

Validation: Rabar H. Faraj.

References

1. Mahasenan, N., Smith, S., & Humphreys, K. (2003, January). The cement industry and global climate change: current and potential future cement industry CO2 emissions. In Greenhouse Gas Control Technologies-6th International Conference (pp. 995–1000). Pergamon.
2. Yu Q. L. (2019). Application of nanomaterials in alkali-activated materials. In *Nanotechnology in Eco-efficient Construction* (pp. 97–121). Woodhead Publishing.
3. Guo X., Shi H., & Dick W. A. (2010). Compressive strength and microstructural characteristics of class C fly ash geopolymer. Cement and Concrete Composites, 32(2), 142–147.
4. Mehta P. K. (2001). Reducing the environmental impact of concrete. Concrete international, 23(10), 61–66.
5. Mejeoumov G. G. (2007). Improved cement quality and grinding efficiency by means of closed mill circuit modeling. Texas A&M University.
6. Provis J. L., Palomo A., & Shi C. (2015). Advances in understanding alkali-activated materials. *Cement and Concrete Research*, 78, 110–125.
7. Abdel-Gawwad H. A., & Abo-El-Enein S. A. (2016). A novel method to produce dry geopolymer cement powder. *HBRC journal*, 12(1), 13–24.
8. Weil M., Dombrowski K., & Buchwald A. (2009). Life-cycle analysis of geopolymer. In *Geopolymers* (pp. 194–210). Woodhead Publishing.
9. Davidovits J. (2008). Geoplolymer chemistry and application. institute Geopolymer Saint-Quentin.
10. Diaz E. I., Allouche E. N., & Eklund S. (2010). Factors affecting the suitability of fly ash as source material for geopolymers. Fuel, 89(5), 992–996.
11. Yip C. K., Lukey G. C., Provis J. L., & van Deventer J. S. (2008). Effect of calcium silicate sources on geopolymerisation. Cement and Concrete Research, 38(4), 554–564.
12. Sumesh M., Alengaram U. J., Jumaat M. Z., Mo K. H., & Alnahhal M. F. (2017). Incorporation of nanomaterials in cement composite and geopolymer based paste and mortar–A review. *Construction and Building Materials*, 148, 62–84.
13. ASTM-C618 (1999) Standard specification for coal fly ash and raw or calcined natural pozzolan for use as a mineral admixture in Concretein concrete, ASTM International, West Conshohocken, PA, USA.
14. Yildirim G., Sahmaran M., & Ahmed H. U. (2015). Influence of hydrated lime addition on the self-healing capability of high-volume fly ash incorporated cementitious composites. Journal of Materials in Civil Engineering, 27(6), 04014187.
15. Omer S. A., Demirboga R., & Khushefati W. H. (2015). Relationship between compressive strength and UPV of GGBFS based geopolymer mortars exposed to elevated temperatures. *Construction and Building Materials*, 94, 189–195.
16. Duxson P., Fernández-Jiménez A., Provis J. L., Lukey G. C., Palomo A., & van Deventer J. S. (2007). Geopolymer technology: the current state of the art. *Journal of materials science*, 42(9), 2917–2933.
17. Ravitheja A., & Kumar N. K. (2019). A study on the effect of nano clay and GGBS on the strength properties of fly ash based geopolymers. *Materials Today*: *Proceedings*, 19, 273–276.
18. Neville A. M., & Brooks J. J. (2010). Concrete technology.
19. ASTM C39/C39M (2017) Standard Test Method for Compressive Strength of Cylindrical Concrete Specimens, ASTM International, West Conshohocken, PA, USA.
20. The European Standard BS EN12390-3, 2009, testing on hardned concrete:part-3: compressive strength of test specimens.
21. Hardjito D., Wallah S. E., Sumajouw D. M., & Rangan B. V. (2004). On the development of fly ash-based geopolymer concrete. *Materials Journal*, 101(6), 467–472.
22. Patankar S. V., Jamkar S. S., & Ghugal Y. M. (2013). Effect of water-to-geopolymer binder ratio on the production of fly ash based geopolymer concrete. *Int. J. Adv. Technol. Civ. Eng*, 2(1), 79–83.
23. Aliabdo A. A., Abd Elmoaty M., & Salem H. A. (2016). Effect of water addition, plasticizer and alkaline solution constitution on fly ash based geopolymer concrete performance. *Construction and Building Materials*, 121, 694–703.
24. De Vargas A. S., Dal Molin D. C., Vilela A. C., Da Silva F. J., Pavao B., & Veit H. (2011). The effects of Na2O/SiO2 molar ratio, curing temperature and age on compressive strength, morphology and microstructure of alkali-activated fly ash-based geopolymers. Cement and concrete composites, 33(6), 653–660.

25. Singhal D., Junaid M. T., Jindal B. B., & Mehta A. (2018). Mechanical and microstructural properties of fly ash based geopolymer concrete incorporating alccofine at ambient curing. *Construction and building materials*, 180, 298–307.

26. Criado M., Palomo A., & Fernández-Jiménez A. (2005). Alkali activation of fly ashes. Part 1: Effect of curing conditions on the carbonation of the reaction products. Fuel, 84(16), 2048–2054.

27. Topark-Ngarm P., Chindaprasirt P., & Sata V. (2015). Setting time, strength, and bond of high-calcium fly ash geopolymer concrete. *Journal of Materials in Civil Engineering*, 27(7), 04014198.

28. Joseph B., & Mathew G. (2012). Influence of aggregate content on the behavior of fly ash based geopolymer concrete. *Scientia Iranica*, 19(5), 1188–1194.

29. Fang G., Ho W. K., Tu W., & Zhang M. (2018). Workability and mechanical properties of alkali-activated fly ash-slag concrete cured at ambient temperature. *Construction and Building Materials*, 172, 476–487.

30. Vijai K., Kumutha R., & Vishnuram B. G. (2010). Effect of types of curing on strength of geopolymer concrete. *International journal of physical sciences*, 5(9), 1419–1423.

31. Muhammad N., Baharom S., Ghazali N. A. M., & Alias N. A. (2019). Effect of Heat Curing Temperatures on Fly Ash-Based Geopolymer Concrete. *Int. J. Eng. Technol*, 8, 15–19.

32. Ibrahim M., Johari M. A. M., Maslehuddin M., & Rahman M. K. (2018). Influence of nano-SiO2 on the strength and microstructure of natural pozzolan based alkali activated concrete. *Construction and Building Materials*, 173, 573–585.

33. Sarker P. K. (2011). Bond strength of reinforcing steel embedded in fly ash-based geopolymer concrete. *Materials and structures*, 44(5), 1021–1030.

34. Wallah S. E. (2010). Creep behaviour of fly ash-based geopolymer concrete. *Civil Engineering Dimension*, 12(2), 73–78.

35. Olivia M., Sarker P., & Nikraz H. (2008). Water penetrability of low calcium fly ash geopolymer concrete. *Proc. ICCBT2008-A*, 46, 517–530.

36. Barbosa V. F., & MacKenzie K. J. (2003). Thermal behaviour of inorganic geopolymers and composites derived from sodium polysialate. Materials research bulletin, 38(2), 319–331.

37. Van Chanh N., Trung B. D., & Van Tuan D. (2008, November). Recent research geopolymer concrete. In The 3rd ACF International Conference-ACF/VCA, Vietnam (Vol. 18, pp. 235–241).

38. Jindal B. Parveen B., Singhal D., & Goyal A. (2017). Predicting relationship between mechanical properties of low calcium fly ash-based geopolymer concrete. *Transactions of the Indian Ceramic Society*, 76(4), 258–265.

39. Embong R., Kusbiantoro A., Shafiq N., & Nuruddin M. F. (2016). Strength and microstructural properties of fly ash based geopolymer concrete containing high-calcium and water-absorptive aggregate. *Journal of cleaner production*, 112, 816–822.

40. Albitar M., Visintin P., Ali M. M., & Drechsler M. (2015). Assessing behaviour of fresh and hardened geopolymer concrete mixed with class-F fly ash. *KSCE Journal of Civil Engineering*, 19(5), 1445–1455.

41. Jaydeep S., & Chakravarthy B. J. (2013). study on fly ash based geo-polymer concrete using admixtures. *International Journal of Engineering Trends and Technology*, 4(10), 4614–4617.

42. Chithambaram S. J., Kumar S., Prasad M. M., & Adak D. (2018). Effect of parameters on the compressive strength of fly ash based geopolymer concrete. *Structural Concrete*, 19(4), 1202–1209.

43. Golafshani E. M., Behnood A., & Arashpour M. (2020). Predicting the compressive strength of normal and High-Performance Concretes using ANN and ANFIS hybridized with Grey Wolf Optimizer. Construction and Building Materials, 232, 117266.

44. George U. A., & Elvis M. M. (2019). Modelling of the mechanical properties of concrete with cement ratio partially replaced by aluminium waste and sawdust ash using artificial neural network. SN Applied Sciences, 1(11), 1514.

45. Mehdipour V., Stevenson D. S., Memarianfard M., & Sihag P. (2018). Comparing different methods for statistical modeling of particulate matter in Tehran, Iran. Air Quality, Atmosphere & Health, 11(10), 1155–1165.

46. Sihag P., Jain P., & Kumar M. (2018). Modelling of impact of water quality on recharging rate of storm water filter system using various kernel function based regression. Modeling earth systems and environment, 4(1), 61–68.

47. Shahmansouri A. A., Bengar H. A., & Ghanbari S. (2020). Compressive strength prediction of eco-efficient GGBS-based geopolymer concrete using GEP method. Journal of Building Engineering, 101326.

48. Velay-Lizancos M., Perez-Ordoñez J. L., Martinez-Lage I., & Vazquez-Burgo P. (2017). Analytical and genetic programming model of compressive strength of eco concretes by NDT according to curing temperature. Construction and Building Materials, 144, 195–206.

49. Gholampour A., Mansouri I., Kisi O., & Ozbakkaloglu T. (2020). Evaluation of mechanical properties of concretes containing coarse recycled concrete aggregates using multivariate adaptive regression splines (MARS), M5 model tree (M5Tree), and least squares support vector regression (LSSVR) models. Neural Computing and Applications, 32(1), 295–308.

50. Behnood A., Olek J., & Glinicki M. A. (2015). Predicting modulus elasticity of recycled aggregate concrete using M5′ model tree algorithm. Construction and Building Materials, 94, 137–147.

51. Golafshani E. M., & Behnood A. (2018). Application of soft computing methods for predicting the elastic modulus of recycled aggregate concrete. Journal of cleaner production, 176, 1163–1176.

52. Mohammed A., Rafiq S., Sihag P., Kurda R., & Mahmood W. (2020). Soft computing techniques: systematic multiscale models to predict the compressive strength of HVFA concrete based on mix proportions and curing times. Journal of Building Engineering, 101851.

53. Shahmansouri A. A., Yazdani M., Ghanbari S., Bengar H. A., Jafari A., & Ghatte H. F. (2020). Artificial neural network model to predict the compressive strength of eco-friendly geopolymer concrete incorporating silica fume and natural zeolite. Journal of Cleaner Production, 279, 123697.

54. Behnood A., Verian K. P., & Gharehveran M. M. (2015). Evaluation of the splitting tensile strength in plain and steel fiber-reinforced concrete based on the compressive strength. Construction and Building Materials, 98, 519–529.

55. Salih A., Rafiq S., Sihag P., Ghafor K., Mahmood W., & Sarwar W. (2021). Systematic multiscale models to predict the effect of high-volume fly ash on the maximum compression stress of cement-based mortar at various water/cement ratios and curing times. Measurement, 171, 108819.

56. Zhao R., Yuan Y., Cheng Z., Wen T., Li J., Li F., et al. (2019). Freeze-thaw resistance of class F fly ash-based geopolymer concrete. *Construction and Building Materials*, 222, 474–483.

57. Shehab H. K., Eisa A. S., & Wahba A. M. (2016). Mechanical properties of fly ash based geopolymer concrete with full and partial cement replacement. *Construction and building materials*, 126, 560–565.

58. Wardhono A., Gunasekara C., Law D. W., & Setunge S. (2017). Comparison of long term performance between alkali activated slag and fly ash geopolymer concretes. *Construction and Building materials*, 143, 272–279.

59. Zeng J., Roy B., Kumar D., Mohammed A. S., Armaghani D. J., Zhou J., et al. (2021). Proposing several hybrid PSO-extreme learning machine techniques to predict TBM performance. Engineering with Computers, 1–17.

60. Varaprasad B. S. K. R. J., & Reddy K. N. K. (2010). Strength and workability of low lime fly-ash based geopolymer concrete. *Indian Journal of Science and Technology*, 3(12).

61. Vignesh P., & Vivek K. (2015). An experimental investigation on strength parameters of flyash based geopolymer concrete with GGBS. *International Research Journal of Engineering and Technology*, 2 (2), 135–142.

62. Murlidhar B. R., Bejarbaneh B. Y., Armaghani D. J., Mohammed A. S., & Mohamad E. T. (2020). Application of Tree-Based Predictive Models to Forecast Air Overpressure Induced by Mine Blasting. Natural Resources Research, 1–23.

63. Chindaprasirt P., & Chalee W. (2014). Effect of sodium hydroxide concentration on chloride penetration and steel corrosion of fly ash-based geopolymer concrete under marine site. *Construction and Building Materials*, 63, 303–310.

64. Shaikh F. U. A., & Vimonsatit V. (2015). Compressive strength of fly-ash-based geopolymer concrete at elevated temperatures. *Fire and materials*, 39(2), 174–188.

65. Sastry K. G. K., Sahitya P., & Ravitheja A. (2020). Influence of nano TiO2 on strength and durability properties of geopolymer concrete. *Materials Today: Proceedings*.

66. Çevik A., Alzeebaree R., Humur G., Niş A., & Gülşan M. E. (2018). Effect of nano-silica on the chemical durability and mechanical performance of fly ash based geopolymer concrete. *Ceramics International*, 44(11), 12253–12264.

67. Adak D., Sarkar M., & Mandal S. (2017). Structural performance of nano-silica modified fly-ash based geopolymer concrete. *Construction and Building Materials*, 135, 430–439.

68. Sumajouw D. M. J., Hardjito D., Wallah S. E., & Rangan B. V. (2007). Fly ash-based geopolymer concrete: study of slender reinforced columns. *Journal of materials science*, 42(9), 3124–3130.

69. Gunasekara C., Law D. W., & Setunge S. (2016). Long term permeation properties of different fly ash geopolymer concretes. *Construction and Building Materials*, 124, 352–362.

70. Mehta A., & Siddique R. (2017). Sulfuric acid resistance of fly ash based geopolymer concrete. *Construction and Building Materials*, 146, 136–143.

71. Huang J., Asteris P. G., Pasha S. M. K., Mohammed A. S., & Hasanipanah M. (2020). A new auto-tuning model for predicting the rock fragmentation: a cat swarm optimization algorithm. Engineering with Computers, 1–12.

72. Nuaklong P., Jongvivatsakul P., Pothisiri T., Sata V., & Chindaprasirt P. (2020). Influence of rice husk ash on mechanical properties and fire resistance of recycled aggregate high-calcium fly ash geopolymer concrete. *Journal of Cleaner Production*, 252, 119797.

73. Okoye F. N., Durgaprasad J., & Singh N. B. (2016). Effect of silica fume on the mechanical properties of fly ash based-geopolymer concrete. *Ceramics International*, 42(2), 3000–3006.

74. Okoye F. N., Prakash S., & Singh N. B. (2017). Durability of fly ash based geopolymer concrete in the presence of silica fume. *Journal of cleaner Production*, 149, 1062–1067.

75. Sarker P. K., Haque R., & Ramgolam K. V. (2013). Fracture behaviour of heat cured fly ash based geopolymer concrete. *Materials & Design*, 44, 580–586. https://doi.org/10.1016/j.matdes.2012.08.005

76. Junaid M. T., Kayali O., & Khennane A. (2017). Response of alkali activated low calcium fly-ash based geopolymer concrete under compressive load at elevated temperatures. *Materials and Structures*, 50 (1), 50.

77. Abhilash P., Sashidhar C., & Reddy I. R. (2016). Strength properties of Fly ash and GGBS based Geopolymer Concrete. *International Journal of ChemTech Research*, *ISSN*, 0974–4290.

78. Cui Y., Gao K., & Zhang P. (2020). Experimental and Statistical Study on Mechanical Characteristics of Geopolymer Concrete. *Materials*, 13(7), 1651. https://doi.org/10.3390/ma13071651 PMID: 32252367

79. Bhogayata A. C., & Arora N. K. (2019). Utilization of metalized plastic waste of food packaging articles in geopolymer concrete. *Journal of Material Cycles and Waste Management*, 21(4), 1014–1026.

80. Gomaa E., Sargon S., Kashosi C., Gheni A., & ElGawady M. A. (2020). Mechanical Properties of High Early Strength Class C Fly Ash-Based Alkali Activated Concrete. *Transportation Research Record*, 0361198120915892.

81. Hassan A., Arif M., & Shariq M. (2019). Effect of curing condition on the mechanical properties of fly ash-based geopolymer concrete. *SN Applied Sciences*, 1(12), 1694.

82. Kurtoglu A. E., Alzeebaree R., Aljumaili O., Nis A., Gulsan M. E., Humur G., et al. (2018). Mechanical and durability properties of fly ash and slag based geopolymer concrete. *Advances in Concrete Construction*, 6(4), 345.

83. Nath P., & Sarker P. K. (2017). Flexural strength and elastic modulus of ambient-cured blended low-calcium fly ash geopolymer concrete. *Construction and Building Materials*, 130, 22–31.

84. Okoye F. N., Durgaprasad J., & Singh N. B. (2016). Effect of silica fume on the mechanical properties of fly ash based-geopolymer concrete. *Ceramics International*, 42(2), 3000–3006.

85. Ramujee K., & PothaRaju M. (2017). Mechanical properties of geopolymer concrete composites. *Materials Today*: *Proceedings*, 4(2), 2937–2945.

86. Saravanan S., & Elavenil S. (2018). Strength Properties of Geopolymer Concrete using M Sand by Assessing their Mechanical Characteristics. *ARPN Journal of Engineering and Applied Sciences*, 13 (13), 4028–4041.

87. Vijai K., Kumutha R., & Vishnuram B. G. (2011). Experimental investigations on mechanical properties of geopolymer concrete composites.

88. Vora P. R., & Dave U. V. (2013). Parametric studies on compressive strength of geopolymer concrete. *Procedia Engineering*, 51, 210–219.

89. Mahmood W., Mohammed A., Ghafor K., & Sarwar W. (2020). Model Technics to Predict the Impact of the Particle Size Distribution (PSD) of the Sand on the Mechanical Properties of the Cement Mortar Modified with Fly Ash. Iranian Journal of Science and Technology, Transactions of Civil Engineering, 1–28.

90. Ghafoor M. T., Khan Q. S., Qazi A. U., Sheikh M. N., & Hadi M. N. S. (2020). Influence of alkaline activators on the mechanical properties of fly ash based geopolymer concrete cured at ambient temperature. *Construction and Building Materials*, 121752.

91. Krishnaraja A. R., Sathishkumar N. P., Kumar T. S., & Kumar P. D. (2014). Mechanical behaviour of geopolymer concrete under ambient curing. *International Journal of Scientific Engineering and Technology*, 3(2), 130–132.

92. Kumaravel S. (2014). Development of various curing effect of nominal strength Geopolymer concrete. *Journal of Engineering Science and Technology Review*, 7(1), 116–119.

93. Nagajothi S., & Elavenil S. (2020). Effect of GGBS Addition on Reactivity and Microstructure Properties of Ambient Cured Fly Ash Based Geopolymer Concrete. *Silicon*, 1–10.

94. Das S. K., & Shrivastava S. (2020). Siliceous fly ash and blast furnace slag based geopolymer concrete under ambient temperature curing condition. *Structural Concrete*.

95. Nuruddin M. N., Kusbiantoro A. K., Qazi S. Q., Darmawan M. D., & Husin N. H. (2011). Development of geopolymer concrete with different curing conditions. *IPTEK The Journal for Technology and Science*, 22(1).

96. Silva R. V., De Brito J., & Dhir R. K. (2014). Properties and composition of recycled aggregates from construction and demolition waste suitable for concrete production. Construction and Building Materials, 65, 201–217.

97. Mohammed A., Rafiq S., Sihag P., Kurda R., Mahmood W., Ghafor K., et al. (2020). ANN, M5P-tree and nonlinear regression approaches with statistical evaluations to predict the compressive strength of cement-based mortar modified with fly ash. Journal of Materials Research and Technology, 9(6), 12416–12427.

98. Zeng F., Amar M. N., Mohammed A. S., Motahari M. R., & Hasanipanah M. (2021). Improving the performance of LSSVM model in predicting the safety factor for circular failure slope through optimization algorithms. Engineering with Computers, 1–12.

99. Yu C., Koopialipoor M., Murlidhar B. R., Mohammed A. S., Armaghani D. J., Mohamad E. T., et al. (2021). Optimal ELM–Harris Hawks Optimization and ELM–Grasshopper Optimization Models to Forecast Peak Particle Velocity Resulting from Mine Blasting. Natural Resources Research, 1–16.

100. Mohammed A. S. (2018). Vipulanandan models to predict the electrical resistivity, rheological properties and compressive stress-strain behavior of oil well cement modified with silica nanoparticles. Egyptian journal of petroleum, 27(4), 1265–1273.

101. Cao J., Gao J., Rad H. N., Mohammed A. S., Hasanipanah M., & Zhou J. (2021). A novel systematic and evolved approach based on XGBoost-firefly algorithm to predict Young's modulus and unconfined compressive strength of rock. Engineering with Computers, 1–17.